JOURNAL OF GEOPHYSICAL RESEARCH, VOL. 114, A01205, doi:10.1029/2008JA013449, 2009

On the coupling between the Harang reversal evolution and substorm dynamics: A synthesis of SuperDARN, DMSP, and IMAGE observations

S. Zou,[1] L. R. Lyons,[1] C.-P. Wang,[1] A. Boudouridis,[1] J. M. Ruohoniemi,[2] P. C. Anderson,[3] P. L. Dyson,[4] and J. C. Devlin[4]

Received 2 June 2008; revised 24 September 2008; accepted 15 October 2008; published 14 January 2009.

[1] The Harang reversal is a prominent feature frequently observed in the electric and magnetic field patterns in the high-latitude auroral zone and plays an important role in substorm dynamics. A comprehensive set of instruments, including Super Dual Auroral Radar Network (SuperDARN), Defense Meteorological Satellite Program (DMSP), and Imager for Magnetopause-to-Aurora Global Exploration (IMAGE), is used to investigate the relationship between the Harang reversal and substorms. On the basis of nine events that have been analyzed, we find that the Harang reversal forms and becomes well defined during the growth phase. Azimuthal flows equatorward of the Harang reversal, a majority of which are in the subauroral region, enhance during the growth phase. The observations indicate that subauroral polarization streams (SAPS) and the Harang reversal evolve together as part of the growth phase development of the region 2 current system. Furthermore, the substorm auroral onset is seen to occur quite near the center of the Harang flow shear, which suggests that the substorm upward field-aligned current develops there. After onset, the evolution of convection flows in the vicinity of the Harang region depends strongly on their location relative to that of the onset. SAPS flows equatorward of the Harang reversal suddenly increase at the substorm onset; flow shear east of the auroral onset relaxes after the onset; and poleward flows, part of a clockwise vortex, are observed west of the auroral onset after the onset. These observations demonstrate the strong coupling between the Harang reversal evolution and substorm dynamics and suggest that the nightside region 2 physics is closely related to substorm dynamics.

Citation: Zou, S., L. R. Lyons, C.-P. Wang, A. Boudouridis, J. M. Ruohoniemi, P. C. Anderson, P. L. Dyson, and J. C. Devlin (2009), On the coupling between the Harang reversal evolution and substorm dynamics: A synthesis of SuperDARN, DMSP, and IMAGE observations, *J. Geophys. Res.*, *114*, A01205, doi:10.1029/2008JA013449.

1. Introduction

[2] The Harang discontinuity is the location where the eastward electrojet lies equatorward of the westward electrojet in the same longitudinal plane [*Harang*, 1946; *Heppner*, 1972]. Since the auroral electrojets are essentially Hall currents, the electric fields are expected to be poleward in the eastward electrojet region and equatorward in the westward electrojet region. Therefore, across the Harang discontinuity latitudinally, electric fields and thus $\vec{E} \times \vec{B}$ convection flows should reverse their direction. In terms of convection flows and electric fields, this is not a strict physical discontinuity, but rather a clockwise rotation of these vectors from higher to lower latitudes. Therefore, in this paper, it will be referred to hereafter as the Harang reversal.

[3] The Harang reversal has been studied by using various instruments, such as ground magnetometers [e.g., *Harang*, 1946], low-altitude polar-orbiting satellites [e.g., *Maynard*, 1974], ground-based coherent scatter radars [e.g., *Nielsen and Greenwald*, 1979] and incoherent scatter radars [e.g., *Kamide and Vickrey*, 1983; *Robinson et al.*, 1985]. These observations have revealed that the reversal can be very dynamic in nature. It can cover a few hours of magnetic local time (MLT) in the dusk to premidnight sector, sometimes even extrude into the postmidnight sector, and its latitudinal location is associated with the strength of geomagnetic activity, moving equatorward as the level of activity increases.

[4] The importance of the Harang reversal is in part because of its close relationship to substorms, which are major disturbances of the magnetosphere-ionosphere system and their onset mechanism has been a controversial topic

[1]Department of Atmospheric and Oceanic Sciences, University of California, Los Angeles, California, USA.
[2]Bradley Department of Electrical and Computer Engineering, Virginia Polytechnic Institute and State University, Blacksburg, Virginia, USA.
[3]Center for Space Sciences, University of Texas at Dallas, Richardson, Texas, USA.
[4]School of Engineering and Mathematical Sciences, La Trobe University, Bundoora, Victoria, Australia.

0148-0227/09/2008JA013449$09.00

for the past few decades. Observations that associate the Harang reversal with the substorm onset arc can be traced back to the 1970s. *Nielsen and Greenwald* [1979] used the Scandinavian Twin Auroral Radar Experiment (STARE) radars and all-sky cameras to study the two-dimensional plasma flow near the Harang reversal. They found that the initiation of the substorm onset can either be an existing arc in the Harang reversal or an arc that suddenly appears equatorward of it. *Baumjohann et al.* [1981] later used a combination of STARE and the Scandinavian Magnetometer Array (SMA) to study the current system associated with local auroral breakups. They found that the substorm breakup arcs observed by all-sky cameras occurred slightly equatorward of the Harang reversal and in the region of northwestward directed electric fields, as inferred from ionospheric equivalent currents calculated from the SMA observations. However, *Gjerloev et al.* [2003] showed that an optical substorm onset occurred in the region where overlap of the two electrojets was observed by the FAST spacecraft in the premidnight sector during the proceeding substorm growth phase and concluded that on the basis of this event, future substorm onset will occur in the Harang reversal region.

[5] The above observations suggest a close relationship between substorm onset and the Harang reversal, but the location of substorm onset relative to that of the Harang reversal has not yet been clarified owing to limitations of available observational tools. The fields of view (fov) of the STARE radar pair is $\sim 400 \times 400$ km^2 in the E region, which is quite limited considering the fact that the reversal can cover a few hours of MLT. In addition, the Doppler velocity measured by an E region coherent scatter radar such as STARE does not fully track the $\vec{E} \times \vec{B}$ drift velocity [*Nielsen and Schlegel*, 1985]. Another problem is that although incoherent scatter radars and low-altitude polar-orbiting satellites are able to measure several important physical parameters, such as plasma drift, electric field, and conductivity in the vicinity of the Harang reversal region within a plane perpendicular to the Earth surface, they cannot reveal a broad instantaneous two-dimensional picture, thus making it difficult to distinguish between spatial and temporal variations. Furthermore, ground magnetic field observations cannot often determine the precise locations of ionospheric currents in any given case, because obtaining high spatial resolution ground magnetic field perturbations at the ground is limited by the lack of a densely enough populated network of ground observatories. Finally, as our observations presented in this paper indicate, there can be very low conductivity in the region equatorward of the center of the Harang flow shear and thus a large spatial conductivity gradient near the center of the Harang reversal, making identification of this region by its current signature difficult.

[6] In recent years, the development of the Super Dual Auroral Radar Network (SuperDARN) enables us to image the large-scale ionospheric convection with high temporal resolution ($\sim$1–2 min) [*Greenwald et al.*, 1995; *Ruohoniemi and Baker*, 1998] and this renews the interest in studying the dynamics of the Harang reversal and its relationship to substorms. *Bristow et al.* [2001] used the SuperDARN radars in the Northern Hemisphere to study the nightside convection pattern during the substorm growth and expansion phases. They found that the meridional flows rotate to become more zonally aligned during the growth phase and enhance 10–20 min before the onset, while the flows decrease and return back to being more meridional at onset. These features are consistent and repeating, thus leading the authors to conclude that there must be a relation between the flow enhancements and the substorm onset. In a following paper, *Bristow et al.* [2003] presented a more detailed analysis of an isolated substorm using a comprehensive set of instruments and found that, during the growth phase, the breakup arcs were equatorward of the Harang reversal, which was inferred from the ground magnetometers and from the radar. These observations are further confirmed in a recent paper by *Bristow and Jensen* [2007]. The above observations strongly indicate that there is an important relationship between the substorm onset and the temporal evolution of the Harang reversal.

[7] Theoretically, the generation of the Harang reversal has been attributed to the dawn-dusk pressure asymmetry in the near Earth plasma sheet [*Erickson et al.*, 1991]. As convection increases, energetic particles are transported from the distant tail into the near Earth plasma sheet and energized. When they become sufficiently energetic, the magnetic gradient and curvature drift dominates the $\vec{E} \times \vec{B}$ drift causing ions to drift westward and electrons to drift eastward. Ions are the dominant contributor to plasma pressure within the plasma sheet. Additionally, the magnetotail has a finite width and the dawnside low-latitude boundary layer (LLBL) is not as good a supplier of energetic ions to the plasma sheet as is the distant tail [*Spence and Kivelson*, 1990, 1993]. As a result, a dawn-dusk plasma pressure gradient with higher pressure at dusk is formed. According to the *Vasyliunas* [1970] equation, this azimuthal pressure gradient plus the gradient of flux tube volume, which is roughly radially outward, would generate an upward field-aligned current. This upward field-aligned current requires converging Pederson current and thus converging electric fields in the ionosphere. These converging electric fields add to the convection electric field and give the north-south directed electric fields that form the Harang reversal. This argument is essentially the same as the one used for explaining the generation of the region 2 field-aligned current system. Thus, theoretically, the Harang reversal is intrinsically related to the region 2 current system. However, there have been very few studies on the details of this relationship.

[8] One limitation of the observations of the Harang reversal using Northern Hemisphere SuperDARN radars is that the radar fov in the substorm onset region near midnight did not usually cover much of the lower latitude portion of the auroral oval and the region 2 area during active conditions. In addition, the HF radar backscatter rate is greatly reduced by sudden enhancements of plasma density in the nearby D and E regions resulting from intense auroral precipitation, which occurs, for example, during substorm expansions and storms [*Milan et al.*, 1999]. In this study, we choose the Southern Hemisphere SuperDARN radars of the Tasman International Geospace Environment Radar (TIGER) project, one in Tasmania and the other in New Zealand. Both radars are located at $\sim -55^\circ$ geomagnetic latitude (mlat), which is $\sim 5^\circ$ lower than the lowest latitude SuperDARN radars in the Northern Hemisphere used in earlier studies. The advantage of the TIGER radar pair lies not only in their capability of imaging the convection flows through-

out the aurora oval, including its lower latitude portion, but also in the fact that they are not expected to suffer from the reduction of backscatter rate due to precipitation during the expansion phase of weak and moderate substorms, because the transmitted beam can reach the F region before reaching the latitude region of intense precipitation. Therefore, the TIGER radar pair should be the most ideal instrument for revealing the structure and dynamics of the Harang reversal. *Grocott et al.* [2006] presented a case study of convection flow evolution in the premidnight sector using the TIGER radar pair and observed a well-defined Harang reversal during a period of auroral activity. In these earlier works, the potential mapping technique was used, which fits the high-latitude potential distribution to observations using spherical harmonic expansion [*Ruohoniemi and Baker*, 1998], while we use the merging technique to get true velocity vectors, the details of which will be discussed in the instrumentation section.

[9] Specifically, we address the following questions: where is the substorm onset location relative to that of the Harang reversal? How do the flows evolve during the substorm growth and expansion phases? Do flows at different locations relative to that of the onset show similar or different evolutions after the onset? How is the flow evolution in the Harang reversal region associated with other region 2 features?

[10] In this study we show that an important aspect of the relationship between the Harang reversal and other region 2 features is that large westward flows associated with large poleward electric field, as the equatorward portion of Harang reversal, are actually at or equatorward of the auroral lower latitude boundary. Thus, these flows have the characteristics of subauroral polarization streams (SAPS) [*Foster and Burke*, 2002]. SAPS have been observed to occur at locations where the equatorward (earthward) boundary of the ion precipitation (plasma sheet) is equatorward (earthward) of that of the electron precipitation (plasma sheet) [*Anderson et al.*, 2001]. The generation of SAPS has been attributed to the plasma sheet pressure gradients that generate the region 2 currents, but in the region equatorward of the plasma sheet electrons, where ionospheric conductivities are low so that large electric fields are required to maintain current continuity within the ionosphere [*Southwood and Wolf*, 1978]. These poleward SAPS electric fields in the ionosphere map back to the magnetotail, superpose onto the convection electric field and can drive extremely large flows, e.g., the magnetosphere counterpart of SAPS.

[11] These strong westward flows have also been studied by *Parkinson et al.* [2003, 2005, 2006, 2007] using the TIGER radar located in Tasmania, although in their studies the flows were referred to as auroral westward flow channels (AWFCs). The authors found that AWFCs typically intensify during the substorm expansion phase. Although they were not able to determine from their analyses whether AWFCs occurred during the growth phase or whether they followed onset, they suggested that AWFCs are a fundamental aspect of the substorm process [*Parkinson et al.*, 2006].

[12] In this paper, we investigate the evolution of the convection flows and thus the electric field in the Harang reversal region during substorm growth and expansion phases. The remainder of the paper is organized as follows: first, we introduce the instruments used in this study; second, a case study is shown as an illustration of our event analysis procedure; third, results from a multicase study are presented in a question-oriented approach; finally, the paper ends with summary and conclusions.

2. Instrumentation

2.1. SuperDARN

[13] The SuperDARN radar network is an international collaboration operating high-frequency (HF) coherent radars in both the Northern and Southern Hemispheres [*Greenwald et al.*, 1995; *Chisham et al.*, 2007]. It measures the ionospheric F region convection velocity due to the $\vec{E} \times \vec{B}$ force in the line of sight (los) direction [*Ruohoniemi et al.*, 1987]. Since variations of convection flows directly reflect changes of the electric fields that map from the magnetosphere, the radar measurements can shed light on physical processes that occur deep in the plasma sheet, the large-scale picture of which is difficult to capture by in situ measurements. The fov of a SuperDARN radar extends $\sim 52^\circ$ in azimuth and covers $\sim 10^6$ km^2 of the ionosphere with temporal resolution typically of 2 min.

[14] The fov's of the SuperDARN radars in the Southern Hemisphere are shown in Figure 1 with those of the two TIGER radars filled in yellow. As one can see, the common fov of the two TIGER radars covers an area about 2 h wide in MLT between $\sim -60^\circ$ and $\sim -85^\circ$ mlat. In our study, the radar data processing consists of two parts: first, los velocities from a single radar, which are initially recorded by range, are mapped onto a global grid with nearly uniform grid cell area of $\sim 111 \times 111$ km^2 ($\sim 1^\circ$ in mlat) in geomagnetic coordinates [*Ruohoniemi and Baker*, 1998]. Second, in the overlap region when los velocity measurements from both radars are available, they are merged together to give the true convection vectors. This is crucial for unambiguously determining the two-dimensional pattern of the Harang reversal.

2.2. IMAGE WIC

[15] The Wideband Imaging Camera (WIC) on board the Imager for Magnetopause-to-Aurora Global Exploration (IMAGE) satellite observes auroras in the far ultraviolet (FUV) band, which are mainly excited by electrons but are also known to be able to be excited by protons. The WIC observations show global optical auroral activity with 2 min temporal resolution and spatial resolution as high as 50 km at apogee, and therefore they can be used to determine the time and location of substorm onset [*Frey et al.*, 2004]. Substorm events analyzed in this work are selected when auroral images over the Southern Hemisphere are available and near the common fov of the TIGER radar pair.

2.3. DMSP

[16] The Defense Meteorological Satellite Program (DMSP) satellites have a sun-synchronous near-polar orbit at an altitude of 800–900 km and with periods of about 101 min. The electron and ion spectrometer (SSJ/4) onboard the DMSP satellite measures particle fluxes of precipitating electrons and ions with energies from 30 eV to 30 keV every second. In addition, the ion drift meter measures the ion horizontal drift velocity component perpendicular to the satellite trajectory. Moreover, the magnetometer measure-

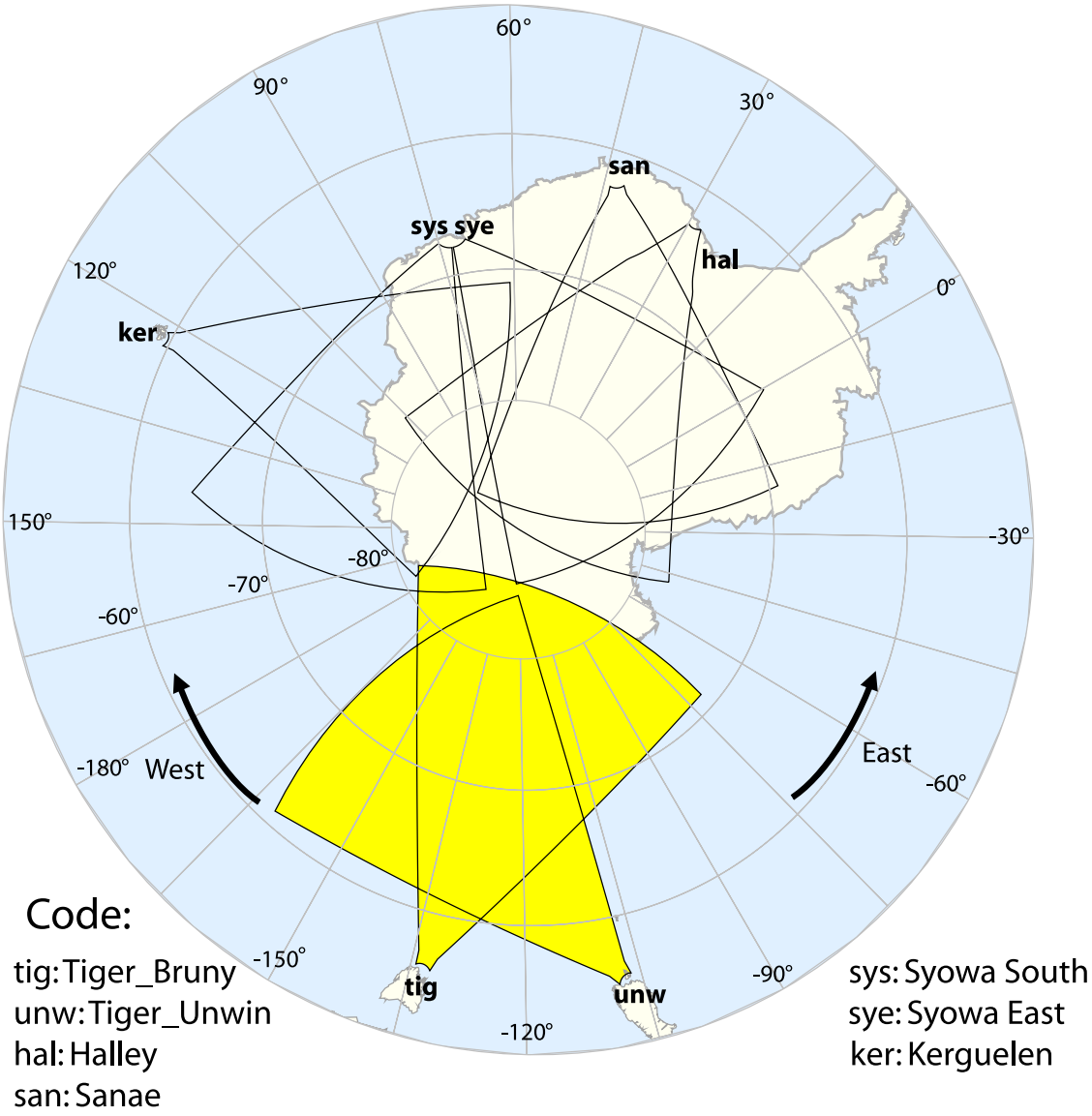

Figure 1. The SuperDARN radar fields of view in the Southern Hemisphere in geomagnetic coordinates, the perspective viewed from above on the Northern Hemisphere. The code of each radar is shown at the bottom. The TIGER_Bruny (tig) and TIGER_Unwin (unw) radar field of view are filled in yellow.

ments can be used to infer the location and direction of any field-aligned currents. The comprehensive measurements from DMSP will be used as a complement to the convection measurements from the TIGER radar pair. The DMSP measurements provide information about the location of electron and ion precipitation boundaries, which allows us to determine the location of the Harang reversal relative to these dynamic boundaries.

[17] This complex set of instruments provides a unique opportunity for us to conduct a comprehensive study of the dynamics of the Harang reversal and its relationship to substorms.

3. Observations

[18] The events analyzed in this study were selected according to the following three criteria: first, sufficient data points are available from both TIGER radars; second, substorm related auroral activity is observed by the IMAGE WIC over the Southern Hemisphere; third, the substorm onset is located near the radar fov. From 1 November 2004, when the TIGER_Unwin radar started to operate (the TIGER_Bruny radar officially started to operate in 2000), to 18 December 2005, when the IMAGE spacecraft lost its communication with the ground controllers, nine substorm events were selected. In addition to the optical aurora signature, other conventional substorm onset signatures, such as energetic particle injections at geosynchronous orbit and low-latitude/midlatitude positive bays, are also used as supportive evidence for substorm onsets.

3.1. Case Study

[19] A substorm on 18 March 2005 was observed by the IMAGE WIC instrument, with initial signature in the 1026:30 UT image shown in Figure 2a. The auroral brightening identified as onset can be seen to be at $\sim -67.5^{\circ}$ mlat

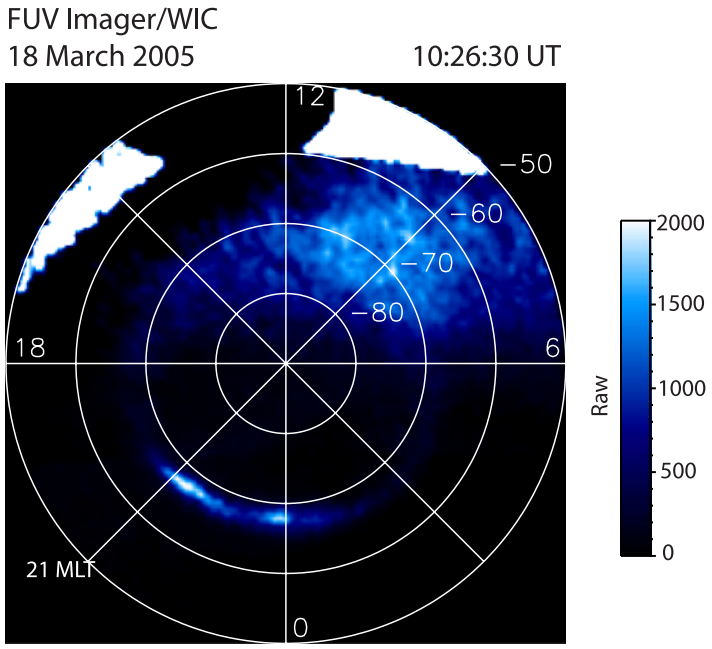

Figure 2a. The IMAGE Wideband Imaging Camera (WIC) observation of a substorm onset at 1026:30 UT on 18 March 2005 in geomagnetic coordinates.

with the maximum luminosity at ~21.3 MLT. Subsequent images (not shown) showed that the aurora brightened further and expanded poleward, indicating that this was a full substorm and not a pseudobreakup. A relatively weaker auroral brightening near midnight can also be seen in this plot, which later images suggest may have been a pseudobreakup.

[20] In Figure 2b, the top shows the energetic proton and electron fluxes measured by Los Alamos National Laboratory satellite 1994−084 with 1 min temporal resolution. At the onset time, the satellite was located near 23.3 MLT. A nearly dispersionless injection signature can be seen in both the proton and electron fluxes. The middle in Figure 2b presents time series of the geomagnetic H component measured by five magnetometers of the Alaska chain, ordered from higher to lower latitudes. Prompt negative and positive excursions reflect the influence of westward and eastward electrojets at substorm onset, respectively. The bottom in Figure 2b shows time series of the nightside geomagnetic H/X component measured by eight low-latitude/midlatitude ground-based magnetometers, in the order of increasing MLT from top to bottom. A positive bay signature is evident in all stations. The onset time based on the particle injections, the magnetic positive bay at low latitude/midlatitude and the magnetic negative bay at auroral latitude is indicated by the black solid line and is consistent with the onset time determined by the IMAGE WIC observations. Lack of activity before and after the onset indicates that this was a clean and isolated substorm, which is ideal for studying the evolution of the convection flow pattern associated with substorms.

[21] The los velocities measured by the TIGER radar pair at 1026−1028 UT are shown from dusk to midnight in geomagnetic coordinates in Figure 3a. Positive values (yellow/red) represent los velocities that are away from the radar and negative values (blue) are velocities toward the radar. The observations combined from the two radars are shown in Figure 3b. The green dotted line, discussed later, approximately indicates the equatorward boundary of the auroral oval. Vectors at points with large squares are merged vectors which are determined by the los velocities from both radars. Vectors at points with small dots are los velocities from only one radar. Vectors point away from the squares (dots) in the direction of the flow (los velocities). Showing both merged and los velocities allows us to see all available flow information in one plot. A strong Harang flow shear, indicated by a yellow line at its center from −110° to −125° longitude, can be identified by flows changing from equatorward and eastward at higher latitudes to westward at lower latitudes. Slightly west of the onset, a flow shear can also be identified by the los velocities from the TIGER_Bruny radar only. However, there was not sufficient data to unambiguously determine whether or not this flow shear was connected with the Harang reversal seen further to the east. The WIC auroral image taken at the substorm onset at 1026:30 UT is superimposed underneath the convection flows in Figure 3b and it can be clearly seen that the substorm onset occurred right at the center of the Harang reversal.

[22] Two DMSP satellites passed near the fov of the radar pair within ~5 min of each other during the growth phase of this substorm. Figures 4a and 4b show observations from DMSP F13 and DMSP F16, respectively. From top to bottom, each panel shows the cross track ion flow velocity (positive values indicating westward flows), the magnetic field perturbations (an increase toward lower latitudes indicating downward field-aligned currents), and the energy spectra of the precipitating electrons and ions. A polar view of the trajectory of each satellite for the period shown is displayed at the upper right corner. In Figures 4a and 4b, the gray vertical solid line indicates the location of the equatorward electron precipitation boundary, which was located at −67.8° mlat and 19.75 MLT as observed by DMSP F13, and

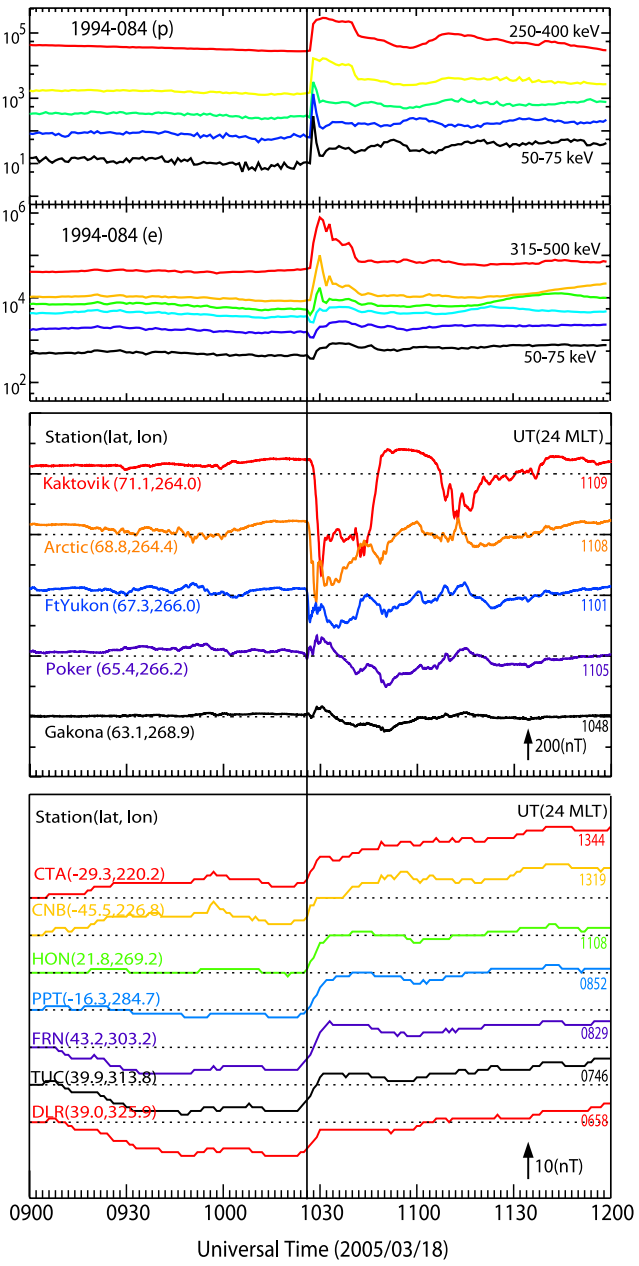

Figure 2b. (top) Energetic proton and electron fluxes observed by Los Alamos National Laboratory satellite 1994–084 from 0900 to 1200 UT on 18 March 2005. The satellite was located at about 23.3 magnetic local time (MLT) at the substorm onset time. (middle) Magnetic H component measured by five magnetometers of the Alaska chain. (bottom) Magnetic positive bay measured by seven low-latitude/midlatitude ground-based magnetometers. The black vertical solid line indicates the substorm onset time.

at −64.7° mlat and 22.23 MLT as observed by DMSP F16. In both cases, the particle observations clearly show that the equatorward boundary of the ion precipitation was further equatorward than that of the electrons. This indicates that, at these local times, the inner edge of the plasma sheet ions was earthward of that of the plasma sheet electrons, which is a necessary condition for the formation of SAPS [*Southwood and Wolf*, 1978]. In the top of Figures 4a and 4b, strong westward flows were indeed observed in the region equatorward of the electron precipitation, consistent with the properties of SAPS.

[23] The magnetic field perturbation ΔB_z displayed in the second panel of Figures 4a and 4b is seen to start to increase toward lower latitudes right from the equatorward boundary of the electron precipitation, which indicates the existence of a downward field-aligned current as indicated by a downward arrow. The magnitude of the slope reflects the intensity of the field-aligned current. The strength of the downward field-aligned current was stronger at the earlier local time observed by DMSP F13 than that at the later local time observed by DMSP F16, indicating spatial inhomogeneity of the current distribution. That SAPS were observed within the region of the downward field-aligned current is in agreement with previous observations [*Anderson et al.*, 2001; *Parkinson et al.*, 2007] and consistent with the original proposal for the SAPS formation [*Southwood and Wolf*, 1978].

[24] In Figure 5, the trajectories of the two DMSP satellites with unfilled squares as one min markers are superimposed on the convection flows as well as the auroral image near the preonset time when they passed over the premidnight region. The auroral brightening near −69° mlat in the image was short lived and without a concurrent magnetic signature, and may have been a pseudobreakup. Stars indicate the location of the poleward and equatorward boundaries of the electron precipitation observed by DMSP. A magenta dotted curve is drawn smoothly to approximately indicate the location of the equatorward boundary of electron precipitation between the two satellite trajectories. Three important features can be seen from this plot: first, the equatorward boundary of electron precipitation approximately collocates with the 300–400 raw counts measured by the IMAGE WIC, suggesting that the IMAGE WIC observations can be used to estimate the dynamic electron plasma sheet equatorial boundary with 2 min temporal resolution; second, large westward flows with peak velocities of ∼750 m/s can be seen at and just equatorward of the auroral oval lower latitude boundary, indicating the presence of SAPS which is strongly supported by the concurrent DMSP observations of Figure 4; third, the combination of the DMSP and SuperDARN observations suggests that in this case, the SAPS flows extended over at least a 3 h MLT range.

[25] The upward and downward field-aligned currents indicated by the two arrows, in Figures 4a and 4b, are separated by the equatorward boundary of the electron precipitation and are well away from the poleward boundary of the plasma sheet. Therefore they should belong to the region 2 current system. This observation, in addition to the observations showing the existence of SAPS, indicates the development of the region 2 current system during the substorm growth phase.

[26] We now can use a similar method to address the location of the Harang reversal in a dynamic coordinate system, such as relative to the auroral boundary. In Figure 3b, the equatorward auroral boundary at substorm onset inferred from the auroral image is indicated by a green dotted line. Compared with that during the growth phase shown in Figure 5, it has moved slightly equatorward at earlier local times, which probably resulted from the earthward excursion

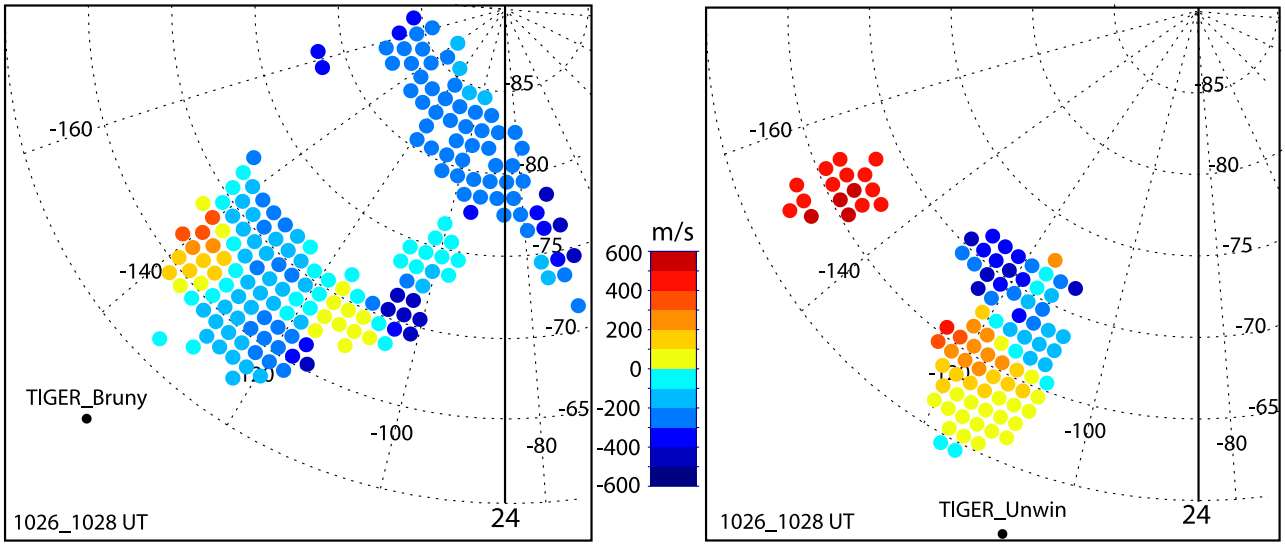

Figure 3a. Line of sight (los) velocities measured by TIGER_Bruny and TIGER_Unwin in the dusk to midnight sector at 1026–1028 UT on 18 March 2005. Each dot represents the location of a los velocity mapped onto a global grid described by *Ruohoniemi and Baker* [1998], and its color represents the direction and magnitude of the los velocity. Blue and negative values mean flows are toward the radar, while yellow/red and positive values mean they are away from the radar.

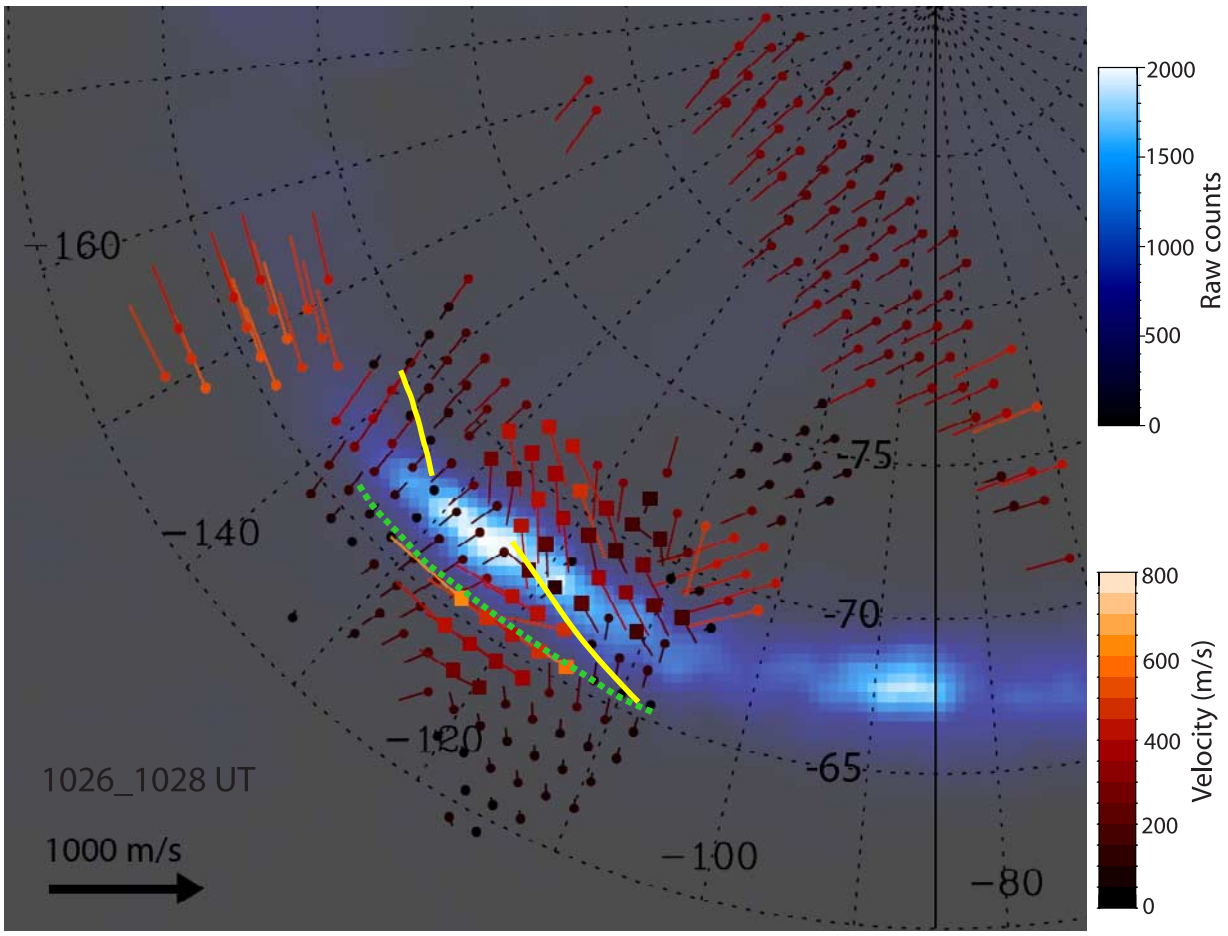

Figure 3b. Convection flows at 1026–1028 UT resulting from the merging procedure superimposed upon the IMAGE WIC observation of a substorm onset at 1026:30 UT. Squares represent merged vectors and dots represent single los velocities. Both the vector's color and length indicate its magnitude, according to the color bar on the right and the reference arrow in the bottom left corner. Yellow lines indicate the center of the Harang reversal. The green dotted line indicates the equatorward boundary of the auroral oval.

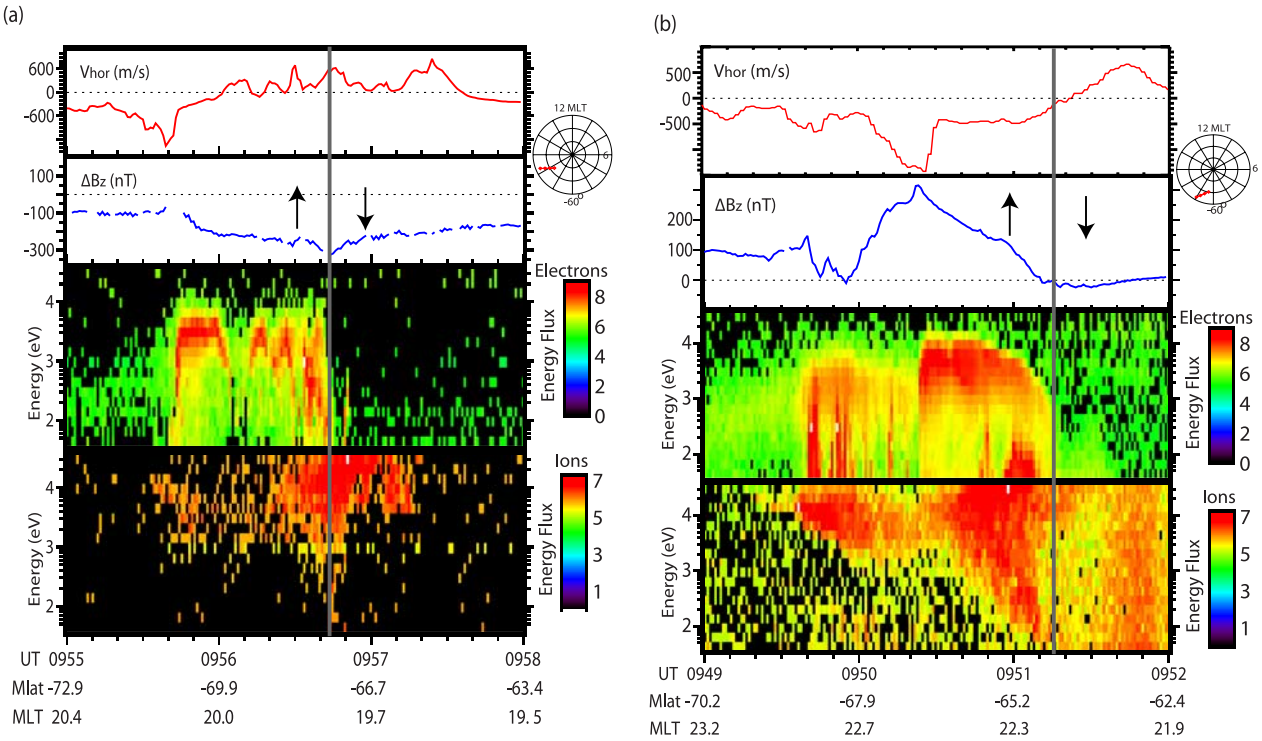

Figure 4. (a) DMSP F13 observations from 0955 to 0958 UT on 18 March 2005. From top to bottom, the plot shows the cross track ion flow speed, the horizontal magnetic field perturbation in the direction normal to the satellite trajectory (an increase toward lower latitudes indicating downward field-aligned currents), and the energy spectra of precipitating electrons and ions. The trajectory of the satellite is shown on the right in a polar view. The solid gray line indicates the equatorward boundary of the electron precipitation. Black arrows indicate the direction of the field-aligned current inferred from the magnetic perturbations. (b) DMSP F16 observations from 0949 to 0952 UT on 18 March 2005, shown in the same format as in Figure 4a.

of the plasma sheet inner edge during the growth phase at that local time. From west to east, the Harang reversal extended from being within the enhanced auroral precipitation region to very near its equatorward boundary. The los velocities from one radar indicate that it extended to higher latitudes further to the west. This implies that the Harang reversal at local times where merged vectors were available was well equatorward of the open-closed field line boundary during this substorm growth phase. The large equatorward/eastward flows at higher latitudes may be an indication of enhanced tail reconnection associated with the substorm growth phase [*de la Beaujardière et al.*, 1994]. In the subauroral region, SAPS are present with peak velocities in excess of ~600 m/s. More importantly, the SAPS comprise most of the westward flows that form the equatorward portion of the Harang reversal. A simultaneous observation of the Harang reversal and SAPS has also been observed during the expansion phase of a substorm [*Grocott et al.*, 2006]. Recently, *Nishimura et al.* [2008] used data from the CRRES spacecraft taken within the premidnight inner magnetosphere and found that the SAPS electric field develops just earthward of the electron plasma sheet. Therefore, the equatorial mapping of the substorm onset, which is just poleward of SAPS in the ionosphere, should be located quite close to the inner edge of the electron plasma sheet.

[27] Using the Chatanika incoherent scatter radar, *Kamide and Vickrey* [1983] studied the variability of the Harang reversal and found that the Hall conductivity poleward of the Harang reversal increased dramatically after a substorm onset. Their observations suggest the existence of upward field-aligned current poleward of the Harang reversal. With the fact that SAPS are collocated with downward field-aligned currents, it seems plausible that the substorm onset on 18 March 2005 occurred also close to the boundary separating the upward and downward region 2 field-aligned currents. This is further supported by the results from a Rice Convection Model (RCM) simulation run, which shows that the center of the Harang reversal is near the boundary of the upward and downward region 2 field-aligned currents [*Gkioulidou et al.*, 2007].

[28] The evolution of the convection flows during the growth and early expansion phases is shown by a set of SuperDARN convection snapshots in Figure 6. Figures 6a–6c are during the growth phase, Figure 6d is at onset, and Figures 6e and 6f are during the early expansion phase. In Figure 6a, westward SAPS and weak equatorward flows poleward of them give a smooth flow shear at the future substorm onset location. These weak equatorward flows progressively rotated to a more eastward direction and kept increasing until the onset. These eastward flows, together with the strong westward flows equatorward of them,

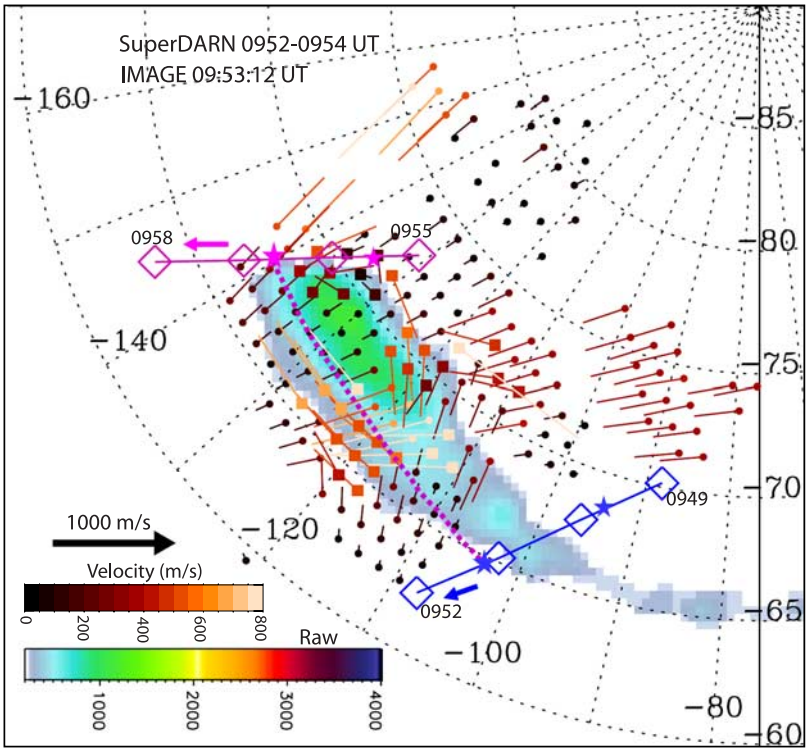

Figure 5. Convection flows at 0952–0954 UT resulting from the merging procedure superimposed upon the IMAGE WIC observation at 0953:12 UT. The trajectories of the two DMSP passes are also shown with squares as 1 min markers. The dotted magenta line roughly represents the location of the equatorward electron precipitation boundary, which is approximately collocated with 300–400 raw counts measured by IMAGE.

formed a very well defined and sharp Harang reversal centered at −67.5° mlat. In the equatorial plasma sheet, the corresponding eastward flows can reduce the loss of energetic ions to the dusk flank of the tail and help to maintain the energetic ions within the plasma sheet and thus also the buildup of the pressure gradient [*Atkinson*, 1984; *Erickson et al.*, 1991]. The observations presented here may indicate that these eastward flows play an important role in substorm dynamics. Additionally, our observations suggest that SAPS formed earlier than the prominent Harang reversal during the growth phase.

[29] After the onset, as shown in Figures 6e and 6f, the enhanced flows poleward of the center of the shear became disturbed and tended to avoid the locally enhanced precipitation region, similar to previous observations [*Yeoman et al.*, 2000; *Bristow et al.*, 2001] and probably related with auroral poleward motion after onset. Unlike the flows poleward of the Harang reversal, the westward flows equatorward of it did not show any discernable change in flow direction.

[30] In order to investigate the magnitude change of these westward flows, their time series are plotted in Figure 7. The black solid curves are the magnitudes of the merged vectors. The dotted lines, color coded according to the same color bar in Figure 6, are results calculated from los velocities measured by a single radar, assuming that the true vectors are parallel to the L shell so that their magnitude can be inferred from

$$|\vec{V}| = \frac{V_{los}}{\cos(\phi)},$$

where ϕ is the angle between the los velocity and the L shell. The good agreement between the black solid lines and the dotted lines suggests that the westward flows roughly maintain their direction during the growth phase. Thus the assumption that the true vectors are nearly parallel to the L shell is appropriate in this situation and can be used to infer the true vectors under similar conditions when los velocities are available from only a single radar. Larger deviations are seen well after the substorm onset, indicating that the flow direction changed at that time. The most striking feature shown in Figure 7 is that right at onset, indicated by the vertical magenta line, the westward flows suddenly increased and reached ~600–700 m/s within about 3–5 min and then leveled off. The observation of flow increase is similar to the observations shown by *Makarevich and Dyson* [2007]. Prompt increase of the electric field in the corresponding region in the inner magnetosphere has also been observed by the in situ CRRES satellite measurements of *Nishimura et al.* [2008]. They found that the SAPS electric field begins to increase within 30 s after the substorm onset. The quick response of the electric fields at onset puts constraints on models explaining the formation of subauroral ion drifts (SAID) after onset, which are based on an average delay of ~10 min after onset [*Galperin*, 2002, and reference therein].

[31] Figure 8 displays the time series of merged convection vectors along the 21.7 MLT meridian, which is slightly east of the center of the onset brightening. Red (blue) arrows represent flow vectors with eastward (westward) components. The length of the vector represents the mag-

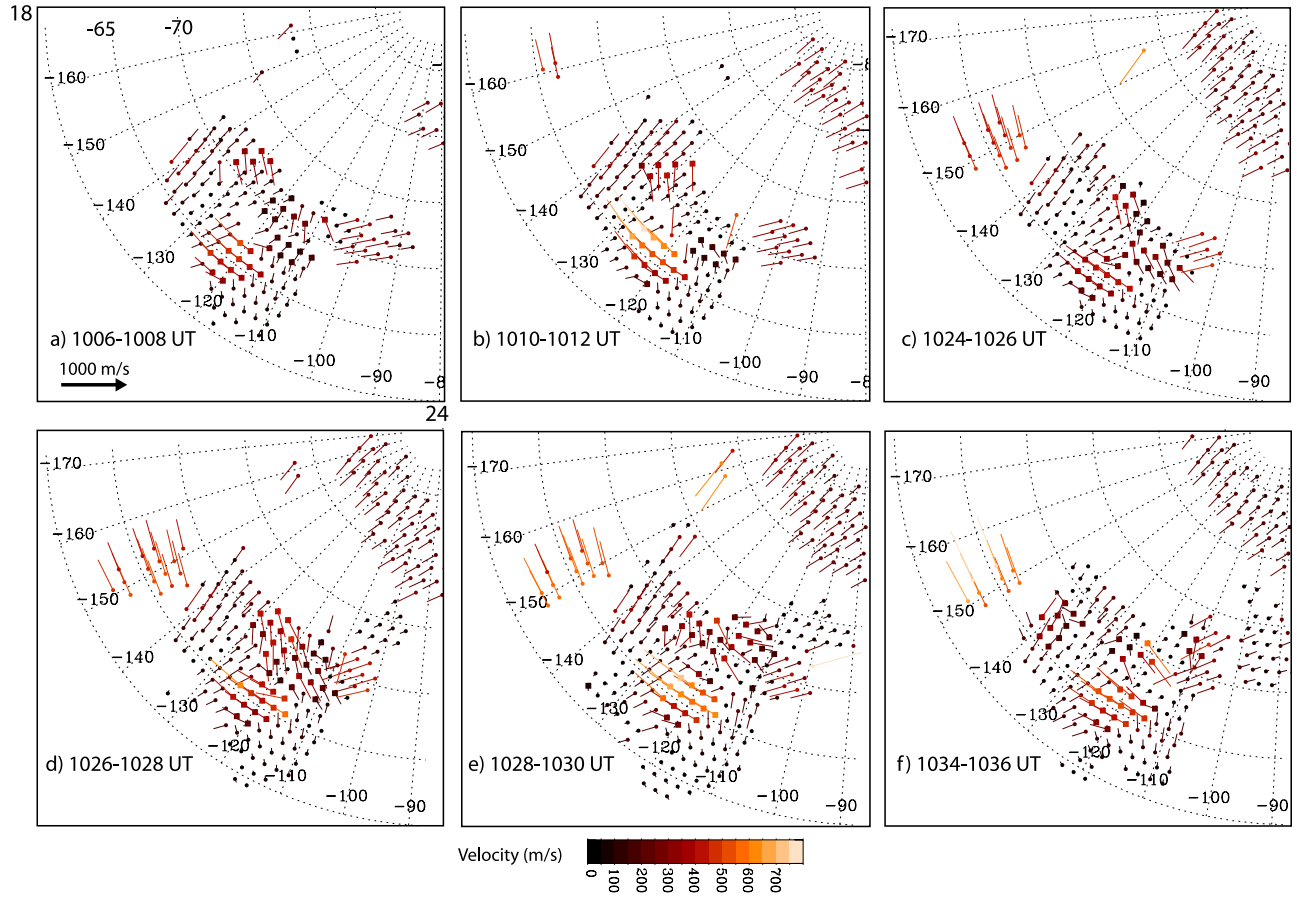

Figure 6. A set of six snapshots of convection flows at specific times. Figures 6a–6c are during the growth phase, Figure 6d is right at onset, and Figures 6e–6f are during the early expansion phase.

nitude of the flow vector and the green solid line indicates the substorm onset time. The observations described in the previous several paragraphs can be roughly summarized in this plot, such as the formation and enhancement of the Harang flow shear during the growth phase, and the enhancement in the westward flows equatorward of the shear after the onset. Another feature we did not cover above is that the convection flows returned back to their quiet time configuration around 1054 UT, which was roughly the end of the recovery phase based on the Alaska magnetometer chain observations taken approximately at the same local time. The main purpose of showing this plot is to introduce its format, since plots similar to this one will be extensively used in the following subsection.

3.2. Multicase Study

[32] Table 1 lists all nine events that have been analyzed in our study. The onset times listed in the second column are based on the WIC observations. The third column lists the available DMSP passes near the radar fov within about an hour before onset. The electron energy spectra observed by DMSP are used to identify the equatorward boundary of the auroral oval. In the first subsection, five out of nine events for which good radar coverage is available at the auroral brightening were selected to address the problem of the substorm onset location relative to that of the Harang reversal and test the generality of what we found in the above example. The following subsection focuses on the evolution of flows at different locations relative to that of the onset after substorm onset.

3.2.1. Substorm Onset Location Relative to That of the Harang Reversal

[33] In order to better understand the substorm onset mechanism, its location has to be accurately determined in "dynamic coordinates," such as relative to the background plasma convection features and to the electron/ion precipitation boundaries. As shown in Figure 3b, the onset on 18 March 2005 occurred right at the center of the Harang flow shear. To examine the generality of this result, Figure 9 shows the observed convection patterns superimposed on the IMAGE WIC observations at substorm onset for the four other events that have relatively good radar data coverage. The Harang reversal is evident in Figures 9a–9d, with its center highlighted by a yellow line. Similar to the first event, the onset brightenings all occurred at the center of the Harang reversal. Because of the poor viewing angle of IMAGE at that time, the auroral image mapped onto the geomagnetic coordinates in Figure 9a is smeared, so the exact onset location cannot be determined without ambiguity. However, the brightest spot is still discernible and is near the center of the Harang reversal. Also, strong westward flows are seen equatorward of the shear center for the three events (Figures 9a–9c) for which merged vectors are available. DMSP passes when available show that these

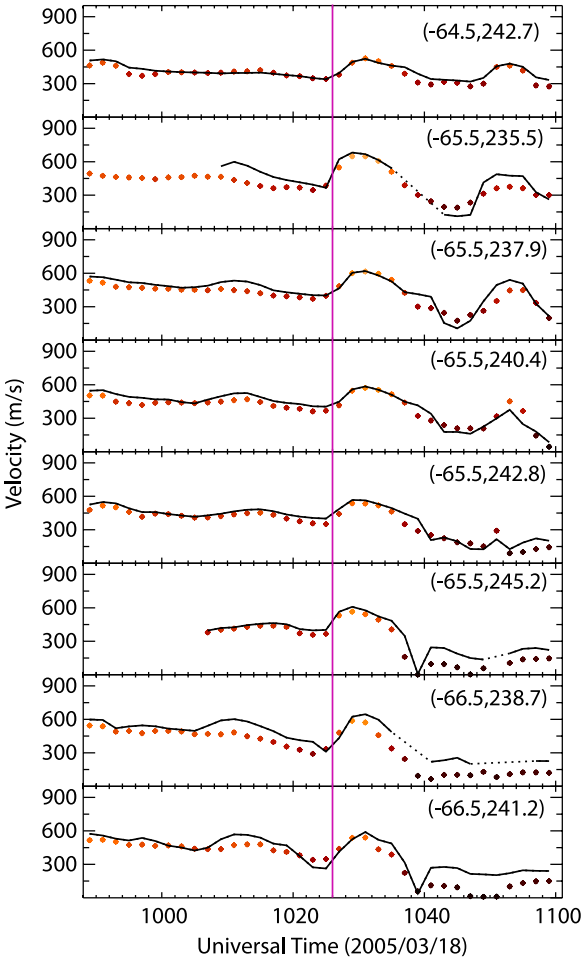

Figure 7. Time series of the magnitude of the westward flows equatorward of the Harang reversal. Black lines represent the magnitudes of the merged vectors, while dotted lines are results calculated from los velocities measured by a single radar, assuming that true vectors are parallel to the L shell. The magenta line indicates the substorm onset time.

Table 1. A List of Nine Substorm Events Analyzed in This Study[a]

Date	Onset Time (UT)	DMSP Passes Near Radar Field of View Before Onset
1 Jan 2005	1238:02	F15 1154 UT 22.6 MLT; F16 1236 UT 21.0 MLT
11 Feb 2005	1045:17	F16 1035 UT 21.7 MLT
16 Feb 2005	1254:46	F15 1154 UT 22.3 MLT
18 Mar 2005	1026:30	F13 0957 UT 19.9 MLT; F16 0951 UT 22.2 MLT
25 Sep 2005	1128:54	F16 1122 UT 22.0 MLT
6 Nov 2005	1117:00	F16 1052 UT 22.2 MLT
12 Nov 2005	1131:23	F16 1118 UT 22.0 MLT
15 Nov 2005	1142:00	F15 1105 UT 22.9 MLT
3 Dec 2005	1239:53	F15 1131 UT 22.6 MLT; F16 1153 UT 21.9 MLT

[a]The substorm onset times are determined by the IMAGE Wideband Imaging Camera observations. The last column lists the DMSP passes near the radar field of view within about an hour before onset. The electron energy spectra observed by DMSP are used to identify the location of the equatorward boundary of auroral oval.

westward flows occurred where the electron precipitation decreased sharply. This further supports their nature as SAPS. It is also consistent with substorm onset being near the center of the Harang reversal and also being very close to the inner edge of the electron plasma sheet.

3.2.2. Convection Evolution During Different Substorm Phases

[34] Owing to the limited common radar fov and variable availability of the radar backscatter rate, merged vectors usually cannot be calculated throughout the area surrounding the substorm onset region simultaneously and continuously. Therefore, the nine events of our study are divided into three categories on the basis of the location of merged vectors relative to that of the onset. Figures 10, 11, and 12 display the time series of convection vectors as a function of geomagnetic latitude for a specified meridional plane that lies east of, close to, and west of the onset, respectively. In Figures 10–12, the green vertical line indicates the substorm onset time. Although the convection flows vary from one substorm to another, all of the cases analyzed in this paper show formation of the Harang reversal during the growth phase. The strength of the shear varies from case to case, and the magnetic latitude of the center of the shear ranges between −62.5° and −67.5°. The detailed structures of the Harang reversal in the nine events show significant

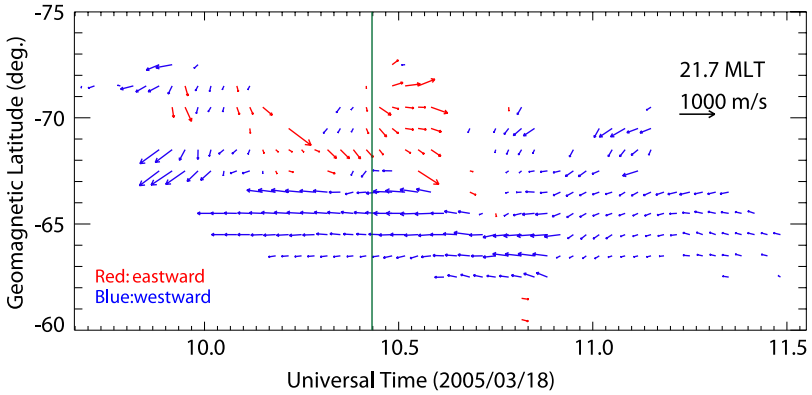

Figure 8. Merged convection vectors from 21.7 MLT as a function of geomagnetic latitude and UT. Red (Blue) arrows represent vectors with eastward (westward) component. The green vertical line indicates the substorm onset time.

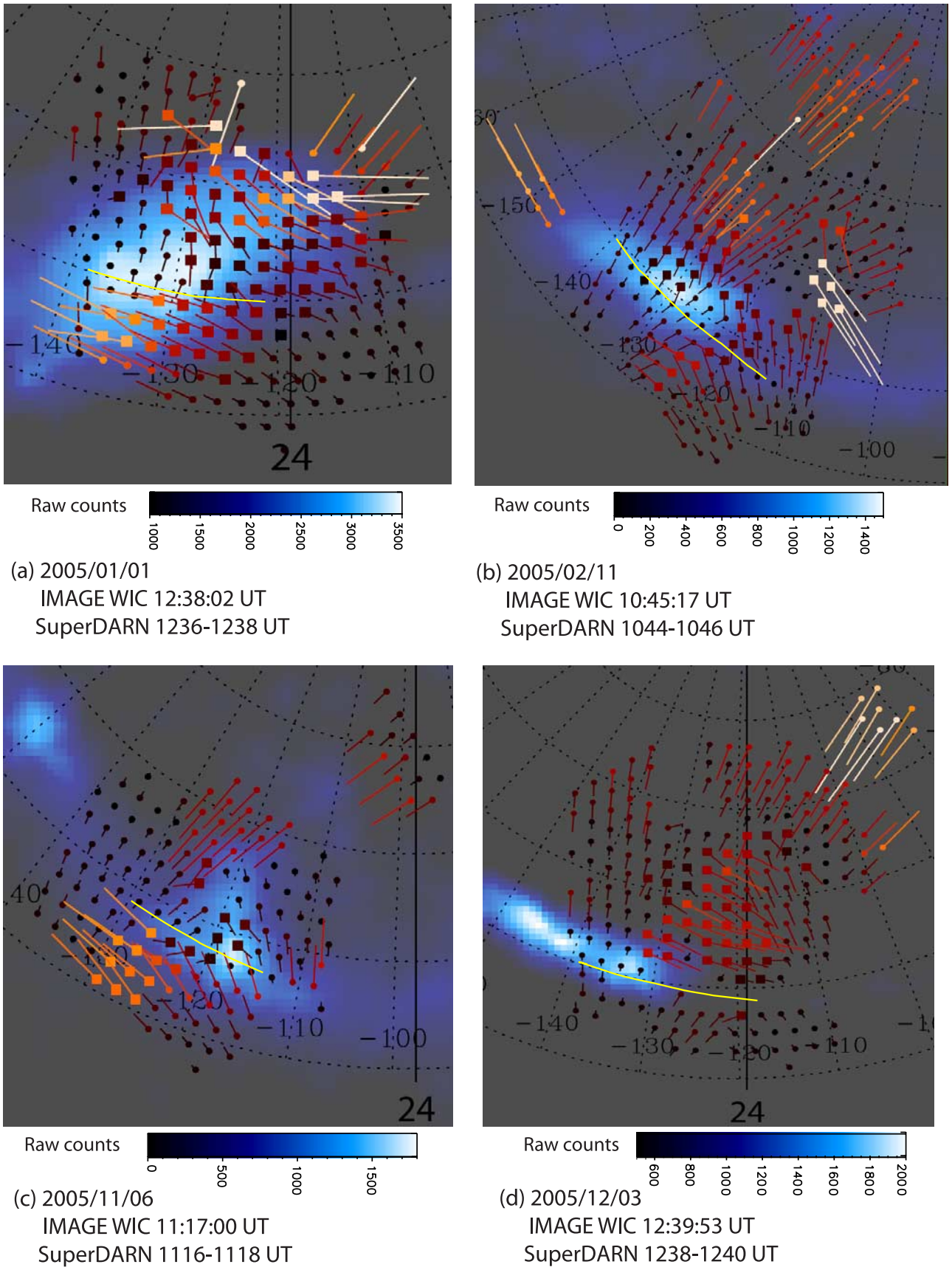

Figure 9. Four more events for which convection flows are available at the onset region, shown in the same format as in Figure 3b. Flow velocities are color coded according to the same color bar in Figure 3b.

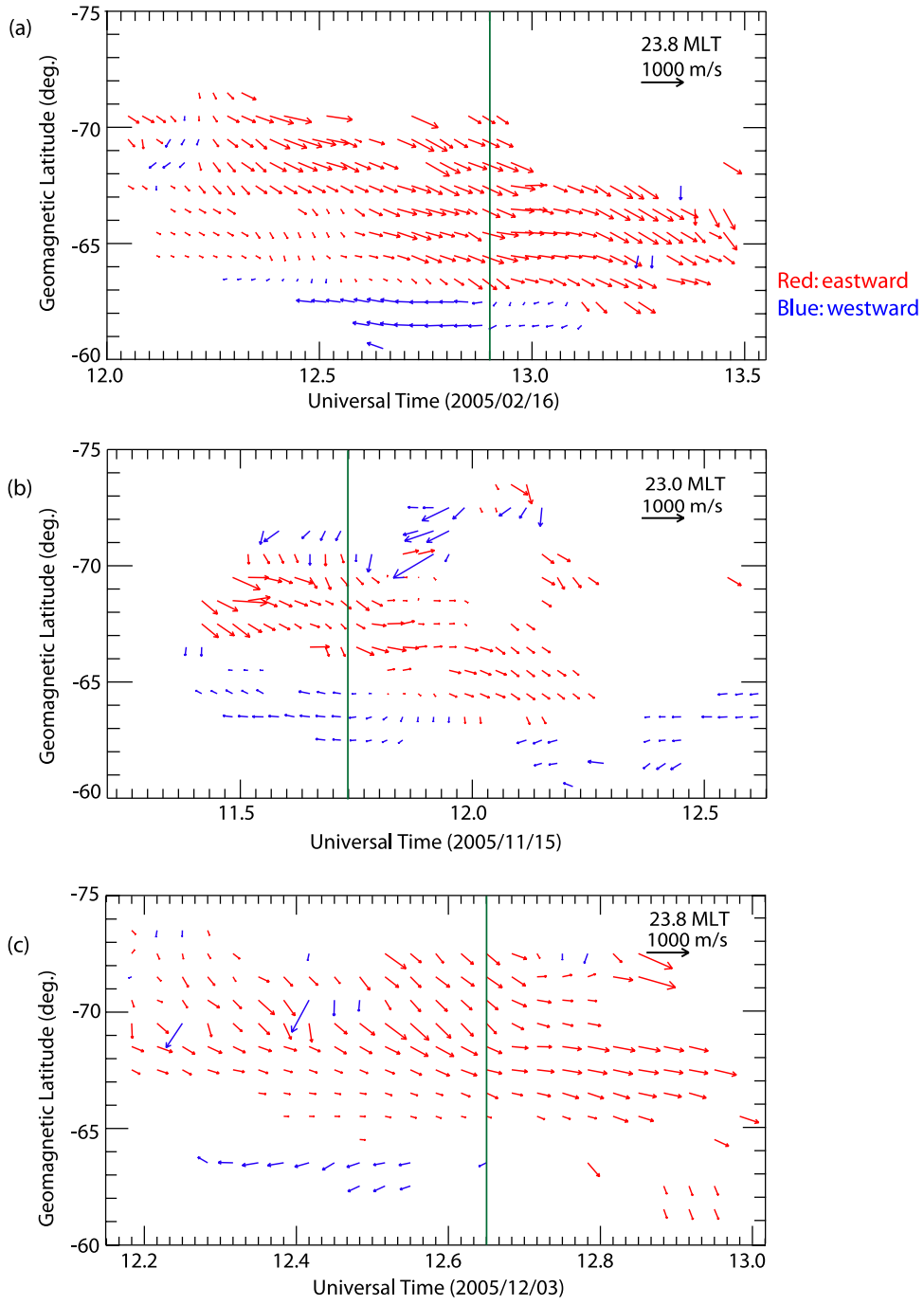

Figure 10. Three events for which the merged vectors are available east of the onset. The format of Figures 10a–10c is the same as in Figure 8.

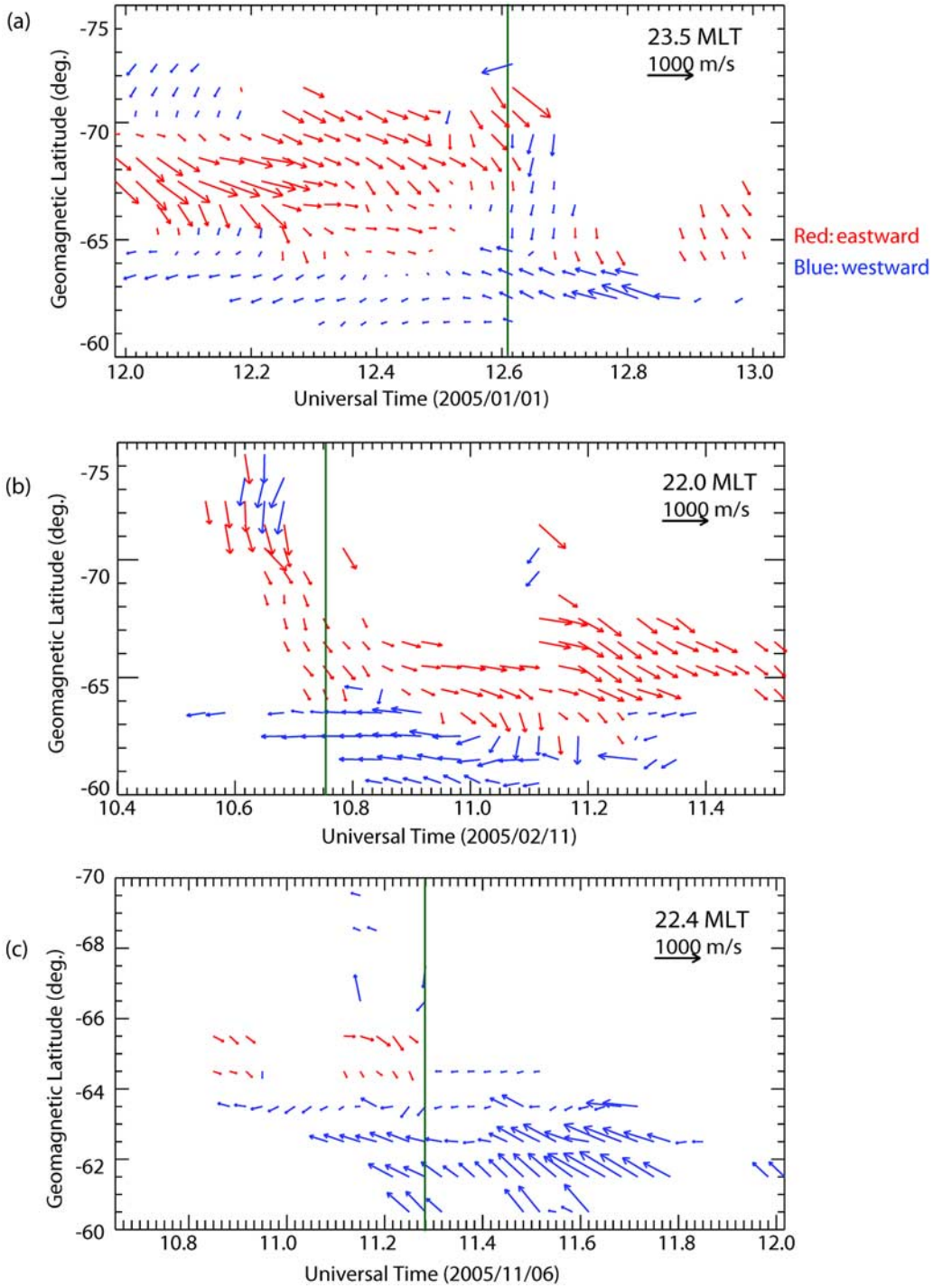

Figure 11. Three events for which the merged vectors are available at the onset. The format of Figures 11a–11c is the same as in Figure 8.

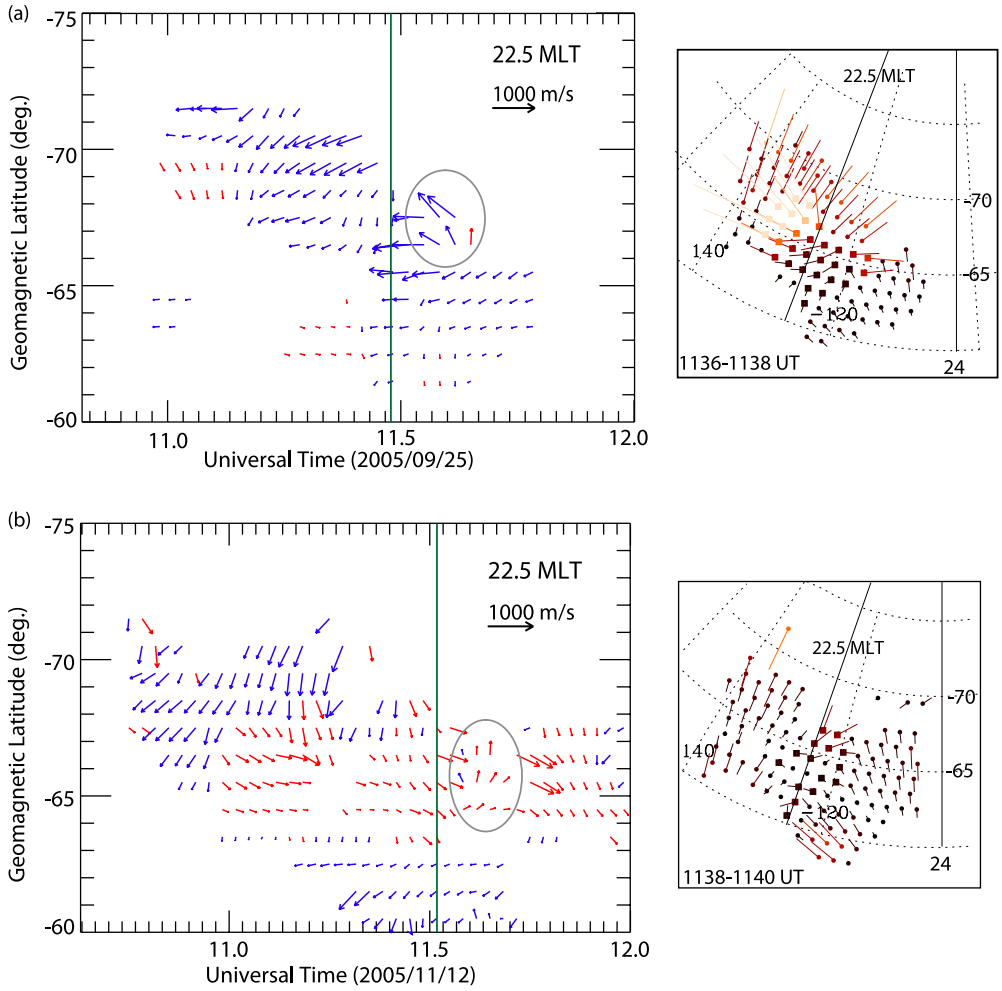

Figure 12. Two events for which the merged vectors are available west of the onset. The format of Figures 12a–12c is the same as in Figure 8. Two-dimensional convection snapshots at the time when poleward flows were observed are available and shown on the right. The color scheme and vector scale length are the same as in Figure 3.

variations, which may be related to the spatial distribution of ionospheric conductivity and the prevailing geomagnetic conditions. In fact, the latter controls the width of the auroral oval and the strength of precipitation, and the conductivity in turn affects the formation of SAPS [*Southwood and Wolf*, 1978]. Therefore, the time scale for the formation of SAPS, and therefore of the Harang reversal, as well as their associated structures, is expected to have significant case-to-case variations.

[35] Figure 10 shows three cases for which the merged vectors are available east of the onset. The meridional planes chosen for the three cases are between 23 and 24 MLT, close to geomagnetic midnight. After the onset, westward flows equatorward of the shear decreased and rotated equatorward to become more meridionally aligned, indicating relaxation of the shear. This is consistent with the results from the potential mapping technique based on observations from the SuperDARN radars in the Northern Hemisphere [*Bristow et al.*, 2001, 2003; *Bristow and Jensen*, 2007]. On the other hand, flows poleward of the shear became more eastward, which might effectively avoid the areas of conductivity enhancement [*Yeoman et al.*, 2000; *Bristow et al.*, 2001] that accompany the poleward and eastward expansion of the auroral precipitation after the onset.

[36] Figure 11 displays convection flows close to the center of the auroral brightening. All three cases show enhancements in the westward flows equatorward of the shear after the onset. Similar to the event on 18 March 2005, two events show a quite quick response (Figures 11a and 11b). As shown in Figure 11b, the flows at higher latitudes did not show significant changes after the westward flows increased, until the westward flows rotated to become more equatorward around 11 UT. Then the flows at higher latitudes began to rotate to a more eastward direction. This is similar to the cases east of the onset shown in Figure 10, and may be related to westward motion of the auroral surge.

[37] Merged vectors chosen from a meridian west of the onset are shown in Figure 12. In both cases, poleward flows are seen during the expansion phase. Two-dimensional distributions of the convection flow at the time when the poleward flows were observed are available and examples are shown on the right side of Figure 12. As one can see, in both cases, the poleward flows were actually a portion of a

clockwise vortex. These clockwise vortices indicate converging electric fields and thus converging Pedersen currents, which are expected to feed upward field-aligned currents coming out of the ionosphere from the center of the vortices. *Opgenoorth et al.* [1983] used the STARE radars and the SMA magnetometer arrays to study the current flows in the vicinity of the surge. They observed converging electric fields near the surge and found a counterclockwise vortex using a model of three-dimensional current system. Their results are consistent with our observations, suggesting that the clockwise vortices we observed were associated with the auroral surge.

[38] On the basis of Figures 10–12, it is clear that convection flows and thus electric fields at different locations relative to that of the onset evolve with dramatic differences during the expansion phase.

4. Summary and Conclusions

[39] Since the discovery of the Harang reversal in 1946, some studies have been carried out to investigate its generation, dynamics and relationship to other geomagnetic disturbances, especially substorms. In our study, we analyzed nine substorm events using a comprehensive set of observational instruments, including the SuperDARN radars, the IMAGE spacecraft, and the DMSP satellites, with the goal of obtaining a relatively complete picture of the Harang reversal evolution during the substorm growth and expansion phases. Additionally, since the underlying physics of the Harang reversal is essentially the same as that of the region 2 field-aligned current system, we also evaluated the relationship between the Harang reversal and other region 2 features, such as field-aligned currents and SAPS. The key observational results are summarized as below and conclusions are drawn on the basis of them.

[40] 1. The Harang reversal is observed during the growth phase of all nine substorms. Its latitudinal location varied between $-67.5°$ and $-62.5°$ geomagnetic latitude. Evidence shows that the shear gradually tilts from higher to lower latitude with increasing MLT, similar to the shape of SAPS [*Foster and Vo*, 2002; *Anderson et al.*, 2001] and it extends from well within the auroral precipitation to its equatorward boundary.

[41] 2. The SAPS region is often seen as the equatorward portion of the Harang reversal during the substorm growth and expansion phases. The magnitude of SAPS flows varies from case to case.

[42] 3. Five cases, for which convection flows are available at the onset location, show that substorm onset occurs right at the center of the Harang flow shear (within the 1° latitudinal spatial resolution), suggesting that the substorm upward field-aligned current at onset comes out of the ionosphere from the center of the Harang flow shear. This substorm onset location is also very close to the equatorward boundary of the electron precipitation (inner edge of the plasma sheet electrons), and to the boundary separating the upward and downward field-aligned currents.

[43] 4. The evolution of the convection flows after onset is found to depend strongly on their location relative to that of the onset. First, westward flows equatorward of the onset, a majority of which are SAPS, further increase after onset. Second, flows east of the onset, closer to magnetic midnight, decrease and rotate equatorward after the onset, relaxing the shear there. Third, poleward flows, part of clockwise vortex, are observed west of onset during the early expansion phase. These observations exhibit the complexity of the physical process in the inner plasma sheet after the substorm onset.

[44] Although every substorm shows certain differences from the others, the observations presented in this paper reveal the above common features of the dynamics of convection flows in the Harang reversal region during substorm growth and expansion phases. This demonstrates that there is a strong coupling between the Harang reversal evolution and substorm dynamics. Our results put constraints on the substorm onset process, and, since the Harang reversal is part of the region 2 electrodynamical system, our results suggest that the nightside region 2 physics is closely associated with substorm dynamics.

[45] **Acknowledgments.** This research was supported at UCLA by National Science Foundation grant ATM-0646233 and NASA grant NNX07AF66. The work by C.-P. Wang was supported by NASA grant NNX07AG42G. The TIGER radars were supported by the Australian Research Council's Discovery Projects (DP0210049, DP0664424) and LIEF Scheme (LE0451713), the Australian Antarctic Science Program, and AFOSR. J. M. Ruohoniemi acknowledges the support of NSF grant ATM-0418101. We thank LANL for providing the energetic particle flux data, the Geophysical Institute of the University of Alaska Fairbanks for providing the Alaska magnetometer data, and the SPIDR Web site for providing the low-latitude and midlatitude magnetometer data. The DMSP particle detectors were designed by Dave Hardy of AFRL, and data were obtained from JHU/APL. We thank Dave Hardy, Fred Rich, and Patrick Newell for its use. We thank Thomas Immel for his help in getting the FUV imager software running at UCLA. We would also like to thank W. A. Bristow for helpful discussions on the topic of this study.

[46] Amitava Bhattacharjee thanks Martin G. Connors and Gareth Chisham for their assistance in evaluating this paper.

References

Anderson, P. C., et al. (2001), Multisatellite observations of rapid subauroral ion drifts (SAID), *J. Geophys. Res.*, *106*, 29,585–29,599, doi:10.1029/2001JA000128.

Atkinson, G. (1984), Thick current sheets in the renovated model of the magnetosphere, *J. Geophys. Res.*, *89*, 8949–8955, doi:10.1029/JA089iA10p08949.

Baumjohann, W., R. J. Pellinen, H. J. Opgenoorth, and E. Nielsen (1981), Joint two-dimensional observations of ground magnetic and ionospheric electric fields associated with auroral zone currents: Current systems associated with local auroral breakup, *Planet. Space Sci.*, *29*, 431–447, doi:10.1016/0032-0633(81)90087-8.

Bristow, W. A., and P. Jensen (2007), A superposed epoch study of SuperDARN convection observations during substorms, *J. Geophys. Res.*, *112*, A06232, doi:10.1029/2006JA012049.

Bristow, W. A., A. Otto, and D. Lummerzheim (2001), Substorm convection patterns observed by the Super Dual Auroral Radar Network, *J. Geophys. Res.*, *106*, 24,593–24,609, doi:10.1029/2001JA000117.

Bristow, W. A., G. Sofko, H. C. Stenbaek-Nielsen, S. Wei, D. Lummerzheim, and A. Otto (2003), Detailed analysis of substorm observations using SuperDARN, UVI, ground-based magnetometers, and all-sky imagers, *J. Geophys. Res.*, *108*(A3), 1124, doi:10.1029/2002JA009242.

Chisham, G., et al. (2007), A decade of the Super Dual Auroral Radar Network (SuperDARN): Scientific achievements, new techniques and future directions, *Surv. Geophys.*, *28*, 33–109, doi:10.1007/s10712-007-9017-8.

de la Beaujardière, O., L. R. Lyons, J. M. Ruohoniemi, E. Friis-Christensen, C. Danielsen, F. J. Rich, and P. T. Newell (1994), Quiet-time intensifications along the poleward auroral boundary near midnight, *J. Geophys. Res.*, *99*, 287–298, doi:10.1029/93JA01947.

Erickson, G. M., R. W. Spiro, and R. A. Wolf (1991), The physics of the Harang discontinuity, *J. Geophys. Res.*, *96*, 1633–1645, doi:10.1029/90JA02344.

Foster, J. C., and W. J. Burke (2002), SAPS: A new categorization for subauroral electric fields, *Eos Trans. AGU*, *83*(36), 393, doi:10.1029/2002EO000289.

Foster, J. C., and H. B. Vo (2002), Average characteristics and activity dependence of the subauroral polarization stream, *J. Geophys. Res.*, *107*(A12), 1475, doi:10.1029/2002JA009409.

Frey, H. U., S. B. Mende, V. Angelopoulos, and E. F. Donovan (2004), Substorm onset observations by IMAGE-FUV, *J. Geophys. Res.*, *109*, A10304, doi:10.1029/2004JA010607.

Galperin, Y. I. (2002), Polarization jet: Characteristics and a model, *Ann. Geophys.*, *20*, 391–404.

Gjerloev, J. W., R. A. Hoffman, E. Tanskanen, M. Friel, L. A. Frank, and J. B. Sigwarth (2003), Auroral electrojet configuration during substorm growth phase, *Geophys. Res. Lett.*, *30*(18), 1927, doi:10.1029/2003GL017851.

Gkioulidou, M., L. R. Lyons, C. Wang, and R. A. Wolf (2007), Effects of plasma sheet condition on the evolution of shielding and the Harang reversal under weak convection: RCM simulations, *Eos Trans. AGU*, *88*(52), Fall Meet. Suppl., Abstract SM13B–1312.

Greenwald, R. A., et al. (1995), DARN/SuperDARN: A global view of the dynamics of high-latitude convection, *Space Sci. Rev.*, *71*, 761–796, doi:10.1007/BF00751350.

Grocott, A., M. Lester, M. L. Parkinson, T. K. Yeoman, P. L. Dyson, J. C. Devlin, and H. U. Frey (2006), Towards a synthesis of substorm electrodynamics: HF radar and auroral observations, *Ann. Geophys.*, *24*, 3365–3381.

Harang, L. (1946), The mean field of disturbance of polar geomagnetic storms, *Terr. Magn. Atmos. Electr.*, *51*(3), 353–380, doi:10.1029/TE051i003p00353.

Heppner, J. P. (1972), The Harang discontinuity in auroral belt ionospheric currents, *Geophys. Norv.*, *29*, 105–120.

Kamide, Y., and J. F. Vickrey (1983), Variability of the Harang discontinuity as observed by the Chatanika radar and the IMS Alaska magnetometer chain, *Geophys. Res. Lett.*, *10*, 159–162, doi:10.1029/GL010i002p00159.

Makarevich, R. A., and P. L. Dyson (2007), Dual HF radar study of the subauroral polarization stream, *Ann. Geophys.*, *25*, 2579–2591.

Maynard, N. C. (1974), Electric field measurements across the Harang discontinuity, *J. Geophys. Res.*, *79*, 4620–4631, doi:10.1029/JA079i031p04620.

Milan, S. E., J. A. Davies, and M. Lester (1999), Coherent HF radar backscatter characteristics associated with auroral forms identified by incoherent radar techniques: A comparison of CUTLASS and EISCAT observations, *J. Geophys. Res.*, *104*, 22,591–22,604, doi:10.1029/1999JA900277.

Nielsen, E., and R. A. Greenwald (1979), Electron flow and visual aurora at the Harang discontinuity, *J. Geophys. Res.*, *84*, 4189–4199, doi:10.1029/JA084iA08p04189.

Nielsen, E., and K. Schlegel (1985), Coherent radar doppler measurements and their relationship to the ionospheric electron drift velocity, *J. Geophys. Res.*, *90*, 3498–3504, doi:10.1029/JA090iA04p03498.

Nishimura, Y., J. Wygant, T. Ono, M. Iizima, A. Kumamoto, D. Brautigam, and R. Friedel (2008), SAPS measurements around the magnetic equator by CRRES, *Geophys. Res. Lett.*, *35*, L10104, doi:10.1029/2008GL033970.

Opgenoorth, H. J., R. J. Pellinen, W. Baumjohann, E. Nielsen, G. Marklund, and L. Eliasson (1983), Three-dimensional current flow and particle precipitation in a westward traveling surge (observed during the Barium-Geos rocket experiment), *J. Geophys. Res.*, *88*, 3138–3152, doi:10.1029/JA088iA04p03138.

Parkinson, M. L., M. Pinnock, H. Ye, M. R. Hairston, J. C. Devlin, P. L. Dyson, R. J. Morris, and P. Ponomarenko (2003), On the lifetime and extent of an auroral westward flow channel (AWFC) observed during a magnetospheric substorm, *Ann. Geophys.*, *21*, 893–913.

Parkinson, M. L., M. Pinnock, J. A. Wild, M. Lester, T. K. Yeoman, S. E. Milan, H. Ye, J. C. Devlin, H. U. Frey, and T. Kikuchi (2005), Interhemispheric asymmetries in the occurrence of magnetically conjugate subauroral polarisation streams, *Ann. Geophys.*, *23*, 1371–1390.

Parkinson, M. L., P. L. Dyson, and M. Pinnock (2006), On the occurrence of auroral westward flow channels and substorm phase, *Adv. Space Res.*, *38*(8), 1755–1762, doi:10.1016/j.asr.2005.08.028.

Parkinson, M. L., J. A. Wild, C. L. Waters, M. Lester, E. A. Lucek, and P. M. E. Décréau (2007), An auroral westward flow channel (AWFC) and its relationship to field-aligned current, ring current, and plasmapause location determined using multiple spacecraft observations, *Ann. Geophys.*, *25*, 59–76.

Robinson, R. M., F. Rich, and R. R. Vondrak (1985), Chatanika radar and S3–2 measurements of auroral zone electrodynamics in the midnight sector, *J. Geophys. Res.*, *90*, 8487–8499, doi:10.1029/JA090iA09p08487.

Ruohoniemi, J. M., and K. B. Baker (1998), Large-scale imaging of high-latitude convection with SuperDARN HF radar observations, *J. Geophys. Res.*, *103*, 20,797–20,811, doi:10.1029/98JA01288.

Ruohoniemi, J. M., R. A. Greenwald, K. B. Baker, J. P. Villain, and M. A. McCready (1987), Drift motions of small-scale irregularities in the high-latitude F region: An experimental comparison with plasma drift motions, *J. Geophys. Res.*, *92*, 4553–4564, doi:10.1029/JA092iA05p04553.

Southwood, D. J., and R. A. Wolf (1978), An assessment of the role of precipitation in magnetospheric convection, *J. Geophys. Res.*, *83*, 5227–5232, doi:10.1029/JA083iA11p05227.

Spence, H. E., and M. G. Kivelson (1990), The variation of the plasma sheet polytropic index along the midnight meridian in a finite width magnetotail, *Geophys. Res. Lett.*, *17*, 591–594, doi:10.1029/GL017i005p00591.

Spence, H. E., and M. G. Kivelson (1993), Contributions of the low-latitude boundary layer to the finite width magnetotail convection model, *J. Geophys. Res.*, *98*, 15,487–15,496, doi:10.1029/93JA01531.

Vasyliunas, V. M. (1970), Mathematical models of magnetospheric convections and its coupling to the ionosphere, in *Particles and Fields in the Magnetosphere*, edited by B. M. McCormac, pp. 60–71, D. Reidel, Hingham, Mass.

Yeoman, T. K., J. A. Davies, N. M. Wade, G. Provan, and S. E. Milan (2000), Combined CUTLASS, EISCAT, and ESR observations of ionospheric plasma flows at the onset of an isolated substorm, *Ann. Geophys.*, *18*, 1073–1087, doi:10.1007/s00585-000-1073-z.

P. C. Anderson, Center for Space Sciences, University of Texas at Dallas, Richardson, TX 75083, USA.

A. Boudouridis, L. R. Lyons, C.-P. Wang, and S. Zou, Department of Atmospheric and Oceanic Sciences, University of California, 405 Hilgard Avenue, Los Angeles, CA 90034, USA. (sha@atmos.ucla.edu)

J. C. Devlin and P. L. Dyson, School of Engineering and Mathematical Sciences, La Trobe University, Bundoora, Vic 3086, Australia.

J. M. Ruohoniemi, Bradley Department of Electrical and Computer Engineering, Virginia Polytechnic Institute and State University, 302 Whittemore Hall, Blacksburg, VA 24061, USA.